Electronic Supplementary Material (ESI) for Nanoscale.

Study of the Nernst effect in 2D materials using first-principles calculations

S. Emad Rezaei and Peter Schindler
Northeastern University, Mechanical and Industrial Engineering Department, Boston, MA, USA
(Dated: January 24, 2024)

I. DENSITY FUNCTIONAL THEORY DETAILS

First- principles density functional theory (DFT) calculations were done based on plane wave self-consistent field (PWscf) and ultrasoft pseudopotential [1] method as treated in the generalized gradient approximation [2] and implemented in Quantum Espresso package (version 7.1) [3]. Brillouin zone was sampled using Monkhorst–Pack scheme. The cutoff energy for the plane-wave-basis set (E_{cut}) and k-mesh were chosen with a convergence threshold for self-consistency of 10^{-8} Ry. DFT input parameters of this article are summarized in Table I. The electron dispersion for each material was graphed along high symmetry k-points, and the conduction bands were shifted to match the experimental band gap. The DFT calculation parameters are provided in Table.I. The experimental lattice constant of 2.464 $\AA$ for carbon family, a = 3.31 $\AA$, and b = 4.37 $\AA$ for phosphorene [4] were taken from literature. A vacuum layer of 15 $\AA$ along c-crystal axis was applied to eliminate the interactions between the 2D layer and its periodic images. The force on atoms along the c-axis was negligible which indicates a vacuum layer of 15 $\AA$ is sufficient. To have localized orbitals, maximally localized Wannier functions were used which represent a successful reproduction of band structures. The Engel–Vosko exchange functional [5] which was employed for band structure calculations includes an improvement factor (F^{ev93}) with a Padé form that is multiplied by LDA-like part of the functional.

$$F^{ev93} = \frac{1 + \alpha_1 g^2 + \alpha_2 g^4 + \alpha_2 g^6}{1 + \beta_1 g^2 + \beta_2 g^4 + \beta_2 g^6} \tag{1}$$

Where $g = |\nabla n|/2nk_F$ and $k_F = \sqrt[3]{(3n\pi^2)}$ are the reduced gradient and the Fermi momentum.

TABLE I. DFT and Wannierization parameters for monolayer graphene (MLG), bilayer graphene (BLG), trilayer graphene (TLG), monolayer phosphorene (MLP), bilayer phosphorene (BLP), and trilayer phosphorene (TLP).

Material	Cutoff energy (Ry)	k-mesh	Wan-mesh	E_g^{wan}(eV)	E_g^{Exp}(eV)
MLG	60	$19 \times 19 \times 1$	200	0.277	0.00
AA-BLG	70	$19 \times 19 \times 1$	300	0.155	0.00
AB-BLG	60	$19 \times 19 \times 1$	260	0.151	0.00
Graphite	60	$19 \times 19 \times 1$	225	0.103	0.00
ABA-TLG	65	$19 \times 19 \times 1$	210	0.015	0.00
ABC-BLG	65	$35 \times 35 \times 1$	180	0.018	0.00
MLP	70	$15 \times 11 \times 1$	320	0.514	1.75
BLP	70	$15 \times 11 \times 1$	290	0.397	1.40
TLP	70	$30 \times 22 \times 1$	180	0.251	1.02

II. FULL BAND STRUCTURES

The full band structures of carbon-family materials and trilayer phosphorene are shown in Figs. 1 and 2, respectively. The effect of van der Waals correction on the band structure of monolayer phosphorene is shown in Fig. 3. This demonstrates that the band structures with and without van der Waals correction are virtually indistinguishable and therefore the van der Waals correction is not expected to affect the calculated Nernst coefficients.

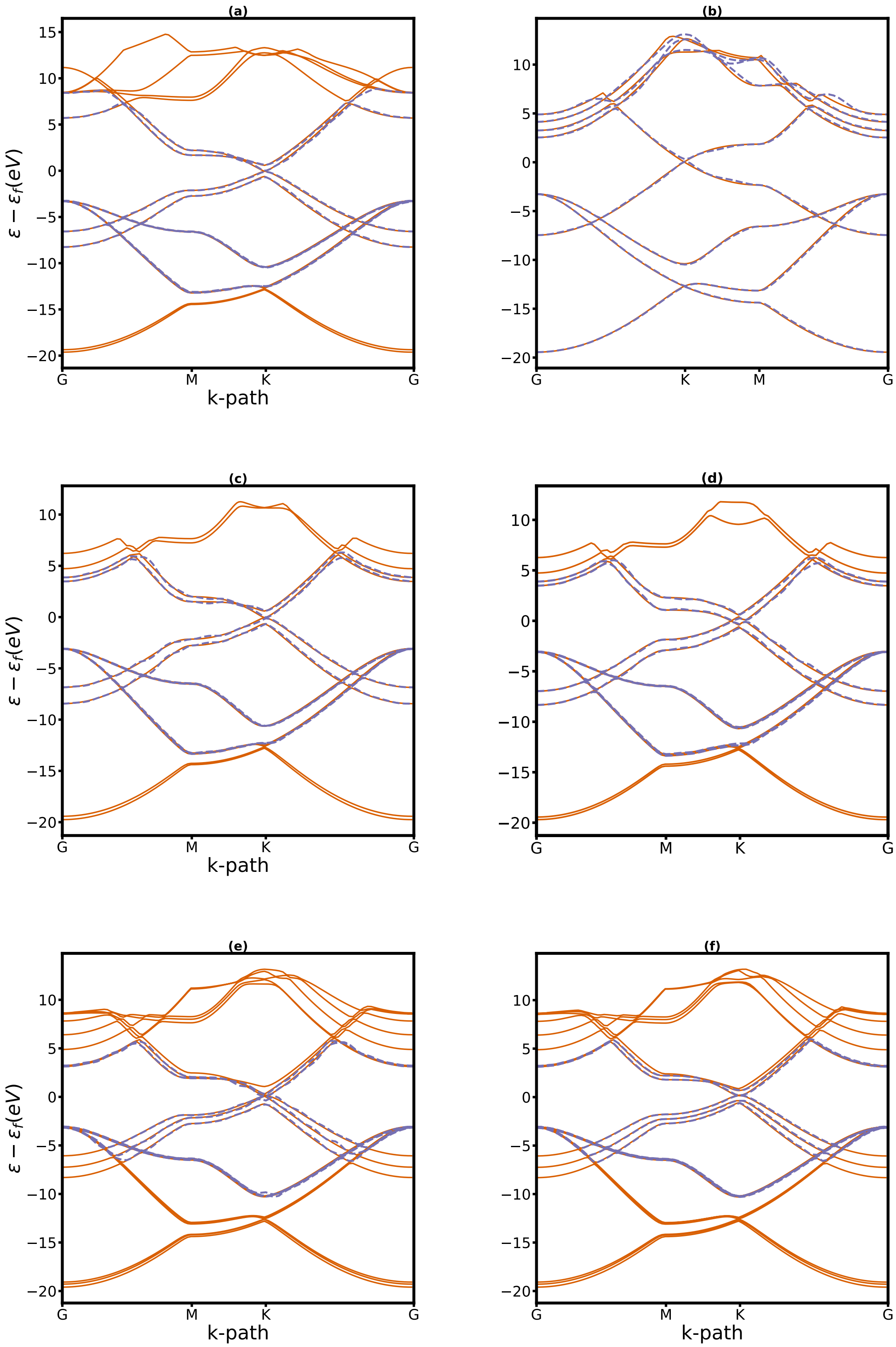

FIG. 1. DFT (orange solid lines) and wannierized (blue dashed lines) structure of graphite (a), monolayer (b), AB stacked bilayer (c), AA stacked bilayer (d), ABA stacked trilayer (e), and ABC stacked trilayer graphene (f). In each case zero is the intrinsic Fermi level.

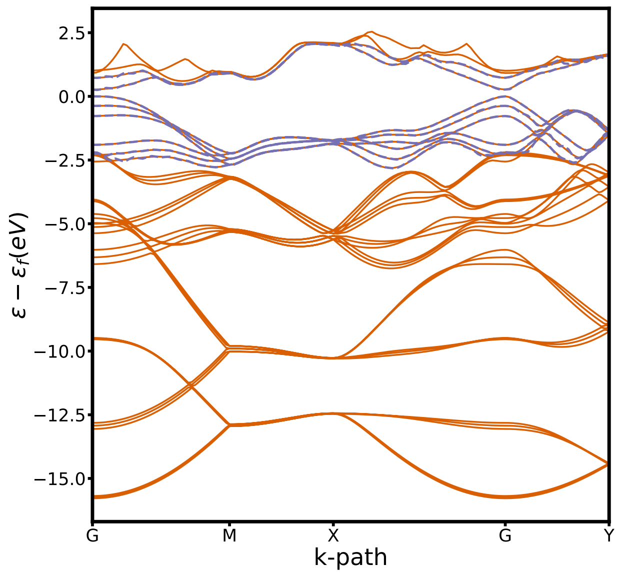

FIG. 2. Wannierized band structure (blue dashed lines) of trilayer phosphorene along with DFT bands (orange solid lines).

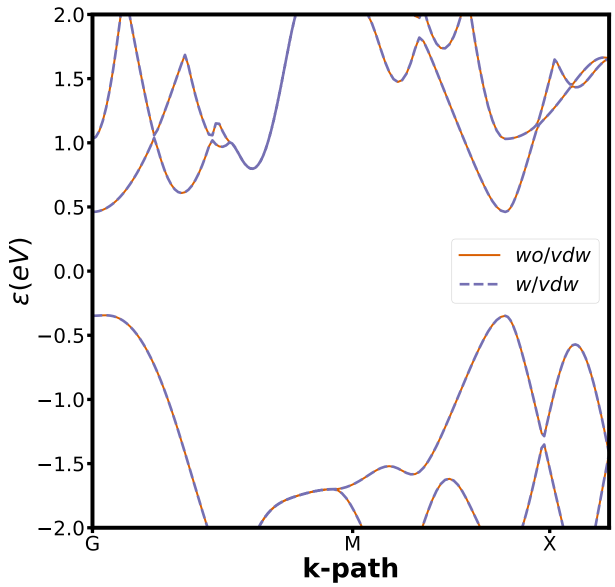

FIG. 3. The band structure of monolayer phosphorene calculated with and without van der Waals correction (blue dashed and orange solid lines, respectively).

III. SCATTERING RATES

Electron-phonon and ionized impurity scattering rates were computed using ElecTra package which requires Fermi surface (carried out by Quantum Espresso) and physical properties of each material. ElecTra code takes various scattering mechanisms into account, namely acoustic phonon deformation potential, polar optical phonons and ionized impurity scattering. The scattering rates' input parameters were adopted from experiments when available; otherwise, we computed them. Table II provides an overview of the input parameters for the materials investigated in this study.

TABLE II. Acoustic ($\mathcal{D}^a$) and optical ($\mathcal{D}^o$) deformation potentials for electrons (e) and holes (h), bulk modulus (**E**), shear modulus (**G**), dielectric constant (ϵ), ionized impurity charge (z), and phonon frequency (ω_{ph}) used in this work.

Material	$\mathcal{D}^a_e$ (eV)	$\mathcal{D}^a_h$ (eV)	$\mathcal{D}^o_e$ (eV/A)	$\mathcal{D}^o_h$ (eV/A)	**E** (Pa)	**G** (Pa)	ϵ	z	ω_{ph} (cm^{-1})
MLG	70 [6]	51 [6]	100 [7]	100 [7]	1×10^{12} [8]	2.8×10^{11} [8]	9.30 [9]	1	1586 [10]
AA-BLG	6.96	7.25	0.93 [11]	2.83 [11]	2×10^{12} [12]	2.205×10^{11} [12]	3.5 [13]	1	1587 [10]
AB-BLG	7.5	5.8	1.01 [14]	2.78 [14]	2.5×10^{12} [15]	1.64×10^{11} [16]	8 [17]	1	1588 [10]
ABA-TLG	4.78	5.01	0.56	1.49	3.25×10^{12} [18]	4.7×10^{11} [18]	6.2 [19]	1	1586 [10]
ABC-TLG	4.15	4.90	0.55	1.47	3.31×10^{12} [20]	1.3×10^{11} [20]	5.4 [19]	1	1586 [10]
Graphite	0.45 [21]	0.50 [21]	0.249 [22]	0.253 [22]	3.8×10^{10} [23]	4.2×10^{9} [23]	17.1508 [9]	1	1582 [10]
MLP	1.33 [24]	1.11 [24]	6.2 [25]	2.2 [25]	1.66×10^{11} [26]	4.1×10^{10} [26]	2.6 [27]	1	438 [28]
BLP	1.40 [24]	1.65 [24]	1.7 [25]	2.28 [25]	1.62×10^{11} [26]	3.8×10^{10} [26]	2.9 [29]	1	441 [28]
TLP	1.51 [24]	1.62 [24]	0.50 [30]	0.42 [30]	1.59×10^{11} [26]	3.7×10^{10} [26]	3.5 [29]	1	439 [28]

[1] D. Vanderbilt, Soft self-consistent pseudopotentials in a generalized eigenvalue formalism, Physical review B **41**, 7892 (1990).

[2] J. P. Perdew, K. Burke, and Y. Wang, Generalized gradient approximation for the exchange-correlation hole of a many-electron system, Physical review B **54**, 16533 (1996).

[3] P. Giannozzi, S. Baroni, N. Bonini, M. Calandra, R. Car, C. Cavazzoni, D. Ceresoli, G. L. Chiarotti, M. Cococcioni, I. Dabo, *et al.*, Quantum espresso: a modular and open-source software project for quantum simulations of materials, Journal of physics: Condensed matter **21**, 395502 (2009).

[4] M. Elahi, K. Khaliji, S. M. Tabatabaei, M. Pourfath, and R. Asgari, Modulation of electronic and mechanical properties of phosphorene through strain, Physical Review B **91**, 115412 (2015).

[5] E. Engel and S. H. Vosko, Exact exchange-only potentials and the virial relation as microscopic criteria for generalized gradient approximations, Physical Review B **47**, 13164 (1993).

[6] C. B. McKitterick, D. E. Prober, and M. J. Rooks, Electron-phonon cooling in large monolayer graphene devices, Physical Review B **93**, 075410 (2016).

[7] R. Shishir and D. Ferry, Intrinsic mobility in graphene, Journal of Physics: Condensed Matter **21**, 232204 (2009).

[8] M. Annamalai, S. Mathew, M. Jamali, D. Zhan, and M. Palaniapan, Elastic and nonlinear response of nanomechanical graphene devices, Journal of Micromechanics and Microengineering **22**, 105024 (2012).

[9] V. M. Pereira, L. G. Hardt, D. G. Fantineli, M. V. Heckler, and L. E. Armas, Characterization of dielectric properties of graphene and graphite using the resonant cavity in 5g test band, Journal of Microwaves, Optoelectronics and Electromagnetic Applications **22**, 63 (2023).

[10] J.-A. Yan, W. Ruan, and M. Chou, Phonon dispersions and vibrational properties of monolayer, bilayer, and trilayer graphene: Density-functional perturbation theory, Physical review B **77**, 125401 (2008).

[11] Y. Chuang, J. Wu, and M. Lin, Electric-field-induced plasmon in aa-stacked bilayer graphene, Annals of Physics **339**, 298 (2013).

[12] Y. Sun, D. Holec, D. Gehringer, O. Fenwick, D. J. Dunstan, and C. Humphreys, Unexpected softness of bilayer graphene and softening of aa stacked graphene layers, Physical Review B **101**, 125421 (2020).

[13] P. Nath, D. Sanyal, and D. Jana, Ab-initio calculation of optical properties of aa-stacked bilayer graphene with tunable layer separation, Current Applied Physics **15**, 691 (2015).

[14] Y. Ge and T. S. Fisher, Photoconductivity calculations of bilayer graphene from first principles and deformation-potential approach, Physical Review B **101**, 235429 (2020).

[15] J.-U. Lee, D. Yoon, and H. Cheong, Estimation of young's modulus of graphene by raman spectroscopy, Nano letters **12**, 4444 (2012).

[16] G. Wang, Z. Dai, Y. Wang, P. Tan, L. Liu, Z. Xu, Y. Wei, R. Huang, and Z. Zhang, Measuring interlayer shear stress in bilayer graphene, Physical review letters **119**, 036101 (2017).

[17] R. Bessler, U. Duerig, and E. Koren, The dielectric constant of a bilayer graphene interface, Nanoscale Advances **1**, 1702 (2019).

[18] M. Huang, P. V. Bakharev, Z.-J. Wang, M. Biswal, Z. Yang, S. Jin, B. Wang, H. J. Park, Y. Li, D. Qu, *et al.*, Large-area single-crystal ab-bilayer and aba-trilayer graphene grown on a cu/ni (111) foil, Nature nanotechnology **15**, 289 (2020).

[19] N. V. Tepliakov, Q. Wu, and O. V. Yazyev, Crystal field effect and electric field screening in multilayer graphene with and without twist, Nano Letters **21**, 4636 (2021).

[20] Z. Gao, S. Wang, J. Berry, Q. Zhang, J. Gebhardt, W. M. Parkin, J. Avila, H. Yi, C. Chen, S. Hurtado-Parra, *et al.*, Large-area epitaxial growth of curvature-stabilized abc trilayer graphene, Nature communications **11**, 546 (2020).

[21] J. Heremans, J.-P. Michenaud, M. Shayegan, and G. Dresselhaus, Magnetostriction and deformation potentials in graphite, Journal of Physics C: Solid State Physics **14**, 3541 (1981).

[22] C. Thomsen, S. Reich, and P. Ordejon, Ab initio determination of the phonon deformation potentials of graphene, Physical Review B **65**, 073403 (2002).

[23] Q. Gao, K. Luo, F. Ling, Q. Huang, Y. Zhang, Q. Han, L. Zhu, Y. Gao, Z. Zhao, B. Xu, *et al.*, Structural determination of a graphite/hexagonal boron nitride superlattice observed in the experiment, Inorganic Chemistry **60**, 2598 (2021).

[24] S. Kaur, A. Kumar, S. Srivastava, K. Tankeshwar, and R. Pandey, Monolayer, bilayer, and heterostructures of green phosphorene for water splitting and photovoltaics, The Journal of Physical Chemistry C **122**, 26032 (2018).

[25] G. Gaddemane, *Theoretical studies of electronic transport in two-dimensional materials for transistor applications*, Ph.D. thesis (2018).

[26] Q. Wei and X. Peng, Superior mechanical flexibility of phosphorene and few-layer black phosphorus, Applied Physics Letters **104** (2014).

[27] E. Kutlu, P. Narin, S. Lisesivdin, and E. Ozbay, Electronic and optical properties of black phosphorus doped with au, sn and i atoms, Philosophical magazine **98**, 155 (2018).

[28] Y. Hong, J. Zhang, and X. C. Zeng, Thermal transport in phosphorene and phosphorene-based materials: A review on numerical studies, Chinese Physics B **27**, 036501 (2018).

[29] P. Kumar, B. Bhadoria, S. Kumar, S. Bhowmick, Y. S. Chauhan, and A. Agarwal, Thickness and electric-field-dependent polarizability and dielectric constant in phosphorene, Physical Review B **93**, 195428 (2016).

[30] B. Liao, J. Zhou, B. Qiu, M. S. Dresselhaus, and G. Chen, Ab initio study of electron-phonon interaction in phosphorene, Physical Review B **91**, 235419 (2015).